International Journal of Nanomedicine

Dovepress
open access to scientific and medical research

Open Access Full Text Article

ORIGINAL RESEARCH

Inhibitory activity of selenium nanoparticles functionalized with oseltamivir on H1N1 influenza virus

This article was published in the following Dove Press journal:
International Journal of Nanomedicine
9 August 2017
Number of times this article has been viewed

Yinghua Li[1]
Zhengfang Lin[1]
Min Guo[1]
Yu Xia[1]
Mingqi Zhao[1]
Changbing Wang[1]
Tiantian Xu[1]
Tianfeng Chen[2]
Bing Zhu[1]

[1]Virus Laboratory, Guangzhou Institute of Pediatrics, Guangzhou Women and Children's Medical Center, Guangzhou Medical University, [2]Department of Chemistry, Jinan University, Guangzhou, People's Republic of China

Abstract: As an effective antiviral agent, the clinical application of oseltamivir (OTV) is limited by the appearance of drug-resistant viruses. Due to their low toxicity and excellent activity, the antiviral capabilities of selenium nanoparticles (SeNPs) has attracted increasing attention in recent years. To overcome the limitation of drug resistance, the use of modified NPs with biologics to explore novel anti-influenza drugs is developing rapidly. In this study, OTV surface-modified SeNPs with superior antiviral properties and restriction on drug resistance were synthesized. OTV decoration of SeNPs (Se@OTV) obviously inhibited H1N1 infection and had less toxicity. Se@OTV interfered with the H1N1 influenza virus to host cells through inhibiting the activity of hemagglutinin and neuraminidase. The mechanism was that Se@OTV was able to prevent H1N1 from infecting MDCK cells and block chromatin condensation and DNA fragmentation. Furthermore, Se@OTV inhibited the generation of reactive oxygen species and activation of p53 phosphorylation and Akt. These results demonstrate that Se@OTV is a promising efficient antiviral pharmaceutical for H1N1.

Keywords: selenium nanoparticles, oseltamivir, influenza virus, neuraminidase, apoptosis

Introduction

The influenza virus is still a serious highly contagious pathogen and affects millions of people in seasonal epidemics.[1–3] H1N1, which belongs to influenza A type viruses, is a highly infectious respiratory disease.[4] Influenza H1N1 was discovered and identified in Mexico in 2009, and resulted in more than 8,768 deaths in 207 countries.[5] There are many ways to spread H1N1 influenza, eg, sneezes, coughs, and contaminated materials. Through rising mutation of the genome and antigenic shifts in different species, the influenza virus has high variability, which may emerge as a novel influenza among humans in the future. There are several steps in the influenza-infection cycle.[6–8] Hemagglutinin (HA) plays an important role in viral infection by combining sialic acid-containing receptors on host cells and mediating the entry and fusion of the virus.[9,10] Neuraminidase (NA) and HA are the most significant glycoproteins on the surface of the influenza virus.[11,12] NA plays an important role in assisting the virus cleave the linkage between sialic acid and HA, when mature viruses separate from the host cell surface.[13] Vaccination is a common method of restraining the spread of influenza infections.[14] Nevertheless, there is a long period between rapid virus evolution and vaccine development.[15] Several antiviral drugs have been developed in the infection cycle. Existing antiviral drugs are amantadine and oseltamivir (OTV).[16] OTV is a transition-state sialic acid analogue against influenza N2 NA,[17] and functions as a

Correspondence: Bing Zhu
Center Laboratory, Guangzhou Women and Children's Medical Center, Guangzhou Medical University, No 318 Renminzhong Road Yuexiu District, Guangzhou 510120, People's Republic of China
Tel +86 20 8133 0740
Fax +86 20 8188 5978
Email: zhubing2016@hotmail.com

Tianfeng Chen
Department of Chemistry, Jinan University, No 601 Huangpu Road, Guangzhou 510120, People's Republic of China
Tel + 86 20 8522 0223
Fax +86 20 8522 1263
Email: tianfengchen2016@hotmail.com

submit your manuscript | www.dovepress.com
Dovepress
http://dx.doi.org/10.2147/IJN.S140939

primary antiviral drug that blocks the release of new virions from cell membranes to afford resistance to influenza A.[18] However, these synthetic drugs have resulted in the emergence of drug-resistant strains, which cause trouble to humans.[19] Therefore, antiviral therapies should promote control of the pandemic influenza A virus.

Due to their unique chemical and physical properties, nanomaterials have emerged as new antimicrobials.[20,21] Pinto et al reported that functionalized multivalent gold nanoparticles (NPs) inhibited the attachment and spread of HSV1.[22] Consensus M2e peptide conjugated to gold NPs presents a promising material against H3N2, H1N1, and H5N1 influenza A viruses.[23] Virus inhibition has been induced by polyvalent NPs of different sizes.[24] Meanwhile, immunization against viral infections by the potential of NPs was reported by Sokolova et al.[25] SiO_2@LDH NPs as an adjuvant to enhance the response of hepatitis B DNA vaccine was reported by Wang et al.[26] Specific interaction for potential bioapplications through efficient encapsulation of Fe_3O_4 NPs into genetically engineered hepatitis B core virus-like particles was reported by Shen et al.[27] In addition, silver NP treatment ameliorates biliary atresia syndrome in rhesus rotavirus-inoculated mice.[28]

Selenium NPs (SeNPs) have attracted considerable attention with their unique antimicrobial activities.[29–31] Selenium is an essential nutritional trace element regulated by cellular redox homeostasis,[32–34] and is an integral component of several selenoproteins that control several crucial biological processes, such as reactive oxygen species (ROS) elimination and specific enzyme modulation.[35–37] A deficiency in selenium can result in susceptibility to infections, including respiratory virus infections.[38] Furthermore, SeNPs have been developed to suppress hepatitis B virus replication and transcription.[39] In this study, we wished to explore novel SeNPs that might interfere with the interaction between H1N1 virus and host cells. We look forward to verifying that OTV-modified SeNPs (Se@OTV) have excellent antiviral activity against H1N1 virus infection. The redox imbalance is associated with many pathologies. The ROS play an important role in many physiological processes.[40,41] An imbalance of redox is implicated in many pathologies, such as cancer, diabetes, and other diseases.[42] Several research groups have described the antimicrobial effects of SeNPs, but reports on their antiviral mechanisms are sparse. Therefore, this study was to investigate whether Se@OTV can reverse H1N1 influenza virus-induced MDCK-cell apoptosis.

Materials and methods

Materials

MDCK cells were obtained from ATCC (CCL-34TM). H1N1 influenza virus was provided by the Virus Laboratory, Guangzhou Institute of Pediatrics, Guangzhou Women and Children's Medical Center, Guangzhou Medical University. FBS and DMEM were obtained from Thermo Fisher Scientific. Akt, PARP, caspase 3, and p53 antibodies were purchased form Cell Signaling Technology. Na_2SeO_3, vitamin C, MTT, propidium iodide, coumarin 6, DAPI, and dichlorofluorescein diacetate (DCF-DA) were purchased from Sigma-Aldrich.

Preparation of Se@OTV

SeNPs were synthesized as follows. Briefly, 0.25 mL of stock solution (0.1 M) of Na_2SeO_3 was gradually added into 2 mL stock solution (50 mM) of vitamin C. Then, 80 μL (100 nM) of OTV was added into the SeNP solution. Excess OTV, vitamin, and Na_2SeO_3 were removed by dialysis for overnight. Se@OTV were sonicated and then filtered through 0.2 μm pores. The concentration of SeNPs and OTV was measured by inductively coupled plasma atomic-emission spectroscopy.

Characterization of Se@OTV

The morphology of Se@OTV was characterized by transmission electron microscopy (TEM; H-7650; Hitachi, Tokyo, Japan). Elemental composition of Se@OTV was determined by energy-dispersive X-ray spectroscopy (EX-250 system; Horiba, Kyoto, Japan). Size distribution and ζ-potential of Se@OTV were monitored by Malvern Zetasizer software. Fourier-transform infrared (FTIR) samples were recorded using the KBr-disk method on an Equinox 55 IR spectrometer. X-ray photoelectron spectroscopy was carried out with an Escalab 250.[43]

Determination of cell viability

The cytotoxicity of Se@OTV was assessed by cell viability as previously described.[44] H1N1 influenza virus was incubated for 2 hours, and virus that had not been internalized was rinsed for removal. OTV with or without SeNPs was added to MDCK cells for 24 hours. Then, MTT (20 μL/well) was added for 5 hours. Formazan crystals were dissolved by adding 150 μL/well dimethyl sulfoxide and recorded at 570 nm absorbance.

Se@OTV-treated H1N1 was detected with TEM.[1] Se@OTV were treated with H1N1 influenza virus and then

attached to a carbon-coated collodion grid. Grids were examined with TEM. MDCK cells were infected with H1N1 for 2 hours. Cell-culture supernatants were harvested after 48 hours, and HA titer measured as previously described.[45] The NA activity of the influenza virus was determined by quantifying the intensity of fluorescence, as previously described.[5]

MDCK cells were confirmed with TUNEL for 1 hour and incubated with DAPI for 15 minutes at 37°C for nuclear staining, as previously described.[46] Fluorescence intensity of caspase-3 activity was detected under fluorescence microscopy with the wavelengths at 380 nm (excitation) and 460 nm (emission), as previously described.[47] TEM analysis of MDCK cells was performed in situ as previously described.[48] ROS levels were monitored by analysis of fluorescence intensity of DCF with 500 nm excitation and 529 nm emission.[49] Se@OTV-treatment influenza on the expression of proteins in MDCK cells was determined as previously reported.[50]

Statistical analysis

All data in this study are presented as means ± SD. Differences with $P<0.05$ or $P<0.01$ were considered statistically significant.

Results and discussion

Preparation of Se@OTV

In this study, we used a simple method to synthesize functionalized SeNPs with OTV on the surface of NPs. SeNPs were modified with OTV to form stabler and more compact globular nanocomposites (Scheme 1). As shown in Figure 1A, due to SeNP modification, the color of SeNPs was deeper than Se@OTV. The Tyndall effect in Se@OTV is shown in Figure 1B and C, and the results indicated that Se@OTV were synthesized.

As shown in Figure 2A, the morphology of Se@OTV presented uniformity spherical particles. As shown in Figure 2B, energy-dispersive X-ray spectroscopy indicated signals of atoms C (20%), O (15%), and N (5%) from OTV, and the percentage of Se atoms was 60%. As shown in Figure 2C and D, Se@OTV decreased from 200 nm to 100 nm, which indicated smaller particles entered cells easily. The ζ-potential of Se@OTV (–36 mV) was lower than SeNPs (–25 mV), demonstrating the higher stability of Se@OTV than SeNPs, as shown in Figure 2E. The size distribution of Se@OTV in Figure 2F revealed that Se@OTV were stable for 30 days. Se@OTV were further characterized by FTIR to confirm the chemical binding of OTV to the surface of the NPs. FTIR spectra of unmodified OTV, SeNPs, and Se@OTV are shown in Figure 3. The FTIR spectrum of Se@OTV resembled that of OTV, giving clear evidence that the OTV ligand formed part of the nanocomposite. OTV displayed IR-absorbance peaks at 3,343 cm^{-1}, 1,720 cm^{-1}, and 752 cm^{-1}, corresponding to $–CH_2$, –C=O, and –C–N. The absence of these peaks in Se@OTV indicated the formation of Se@OTV. X-ray photoelectron-spectroscopy data were also recorded to examine the interaction between OTV and Se@OTV. As shown in Figure 4, the O 1s peak in the spectrum of Se@OTV further confirmed that OTV had been successfully conjugated to the SeNPs.

In vitro antiviral activity of Se@OTV

The cell viability of H1N1 was 36%, and OTV and SeNPs increased viability to 53% and 60%, as shown in Figure 5A. However, the cell viability of Se@OTV was significantly increased to 93%. The results suggest that the antiviral activity of SeNPs was effectively amplified by OTV. As shown in Figure 5B, cells treated with H1N1 showed cytoplasmic shrinkage, loss of cell–cell contract, and reduction in cell numbers. MDCK-cell morphology was changed

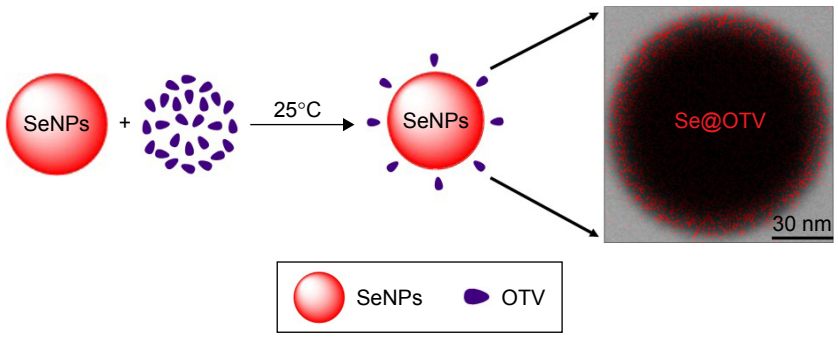

Scheme 1 Synthetic route of Se@OTV.
Abbreviations: SeNPs, selenium nanoparticles; OTV, oseltamivir; Se@OTV, OTV SeNPs.

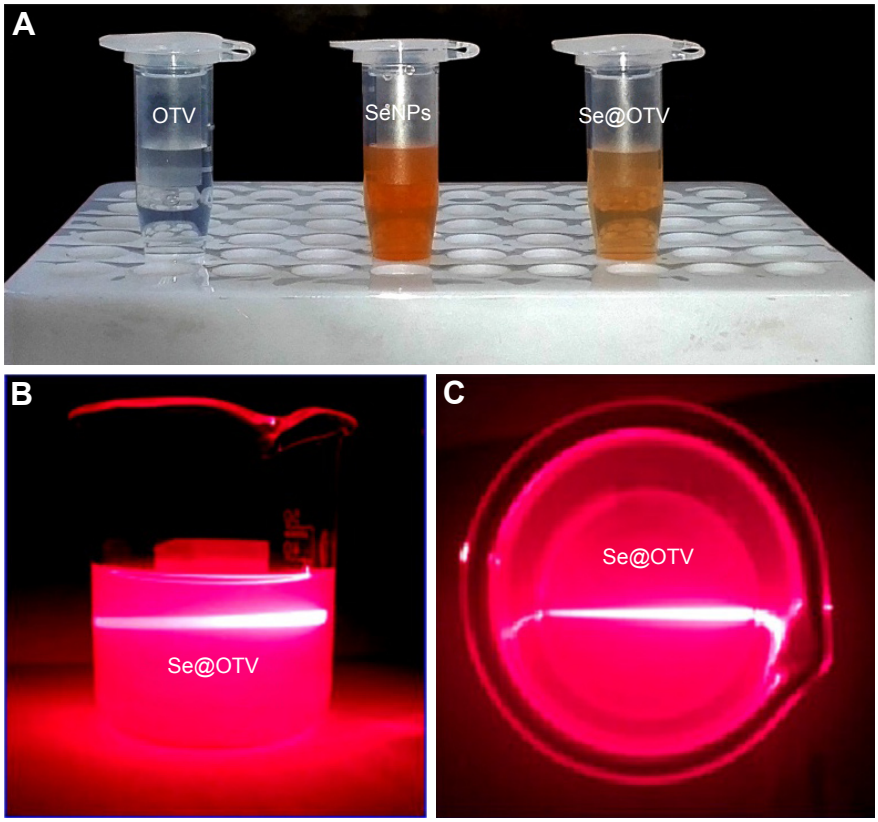

Figure 1 Light images of OTV, SeNPs, and Se@OTV.
Notes: (**A**) Color changes in OTV, SeNPs, and Se@OTV; (**B**, **C**) Tyndall effect in Se@OTV.
Abbreviations: OTV, oseltamivir; SeNPs, selenium nanoparticles; Se@OTV, OTV SeNPs.

slightly by cotreatment with Se@OTV, and appeared healthy, with regularity in shape. Synergy was evaluated by calculation of in vitro fractional inhibitory concentration-index values: minimum inhibitory concentration (MIC) of drug A combination present in Se@OTV of Se (125 μM); MIC of drug B combination present in Se@OTV of OTV (0.3 nM); MIC of drug A alone corresponded to free SeNPs (1 mM); MIC of drug B alone corresponded to free OTV (1 nM).

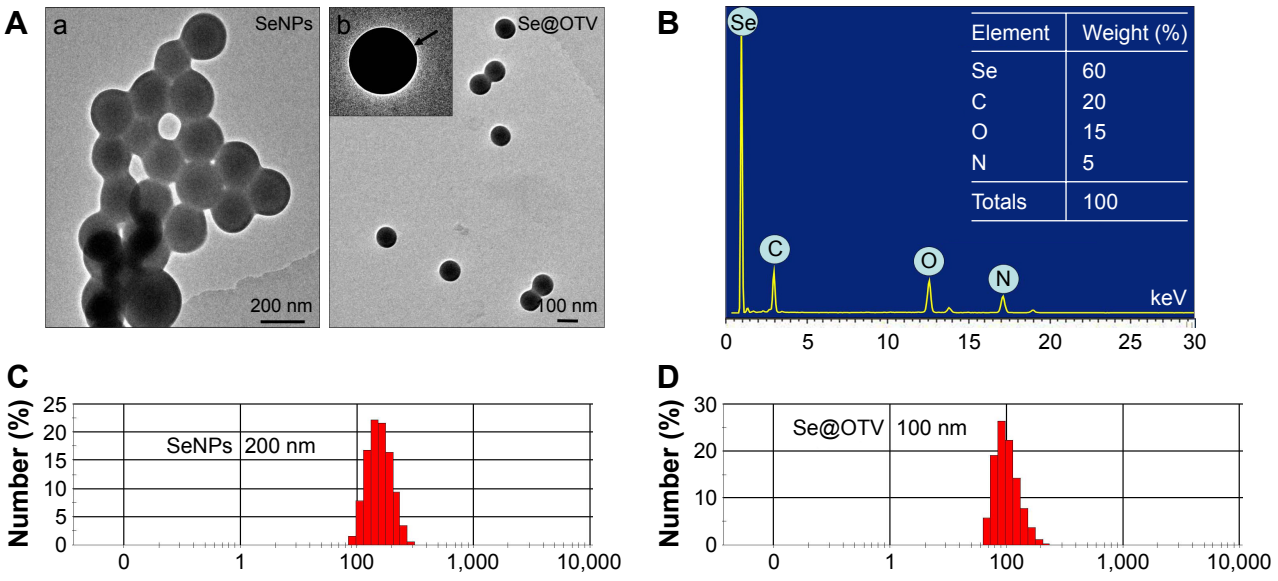

Figure 2 (*Continued*)

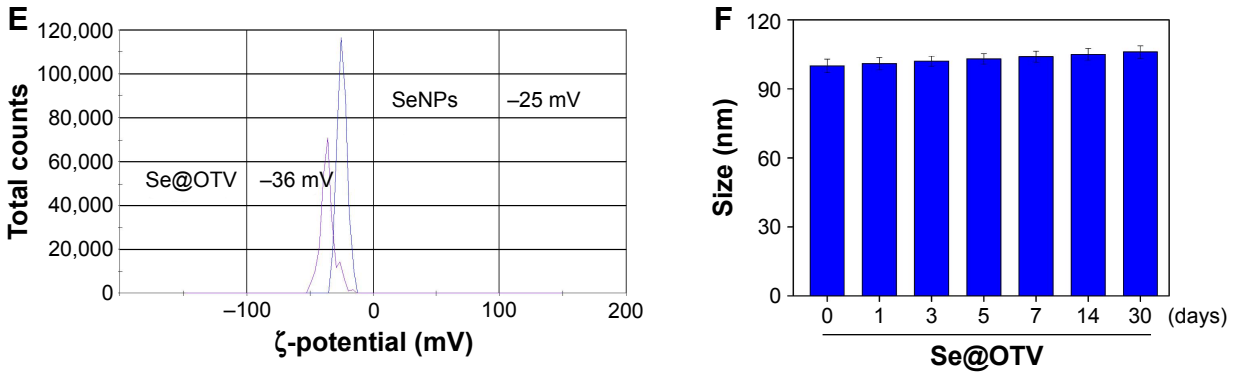

Figure 2 Characterization of SeNPs and Se@OTV.
Notes: (**A**) TEM of (a) SeNPs and (b) Se@OTV; (**B**) EDX analysis of Se@OTV; (**C**, **D**) size distribution of SeNPs and Se@OTV; (**E**) ζ-potential of SeNPs and Se@OTV; (**F**) stability of Se@OTV in aqueous solutions.
Abbreviations: SeNPs, selenium nanoparticles; OTV, oseltamivir; Se@OTV, OTV SeNPs; TEM, transmission electron microscopy; EDX, energy-dispersive X-ray.

Fractional IC (FIC) was calculated as (MIC drug A combination/MIC drug A alone) + (MIC drug B combination/MIC drug B alone) =125 μM/1 mM +0.3 nM/1 nM =0.425. FIC was 0.425, below 0.5, indicating synergy. In this study, the FIC index was basically interpreted as follows: FIC <0.5, synergy; FIC 0.5–2, indifference; FIC >2, antagonism. The results suggest that Se@OTV effectively inhibited the proliferation of H1N1 (Table 1).

H1N1 morphology changes

H1N1-virus control (approximately 50 nm) showed typical elliptical or spherical normal H1N1 containing virus matrix and capsids (Figure 6A). After interaction of Se@OTV with H1N1 for 30 minutes, parts of H1N1 viral edges were lost and viral morphology destroyed (Figure 6B). The results demonstrated that Se@OTV interacted directly with virus particles, leading to disruption of viral function.

Identification of HA and NA by Se@OTV

Compared to OTV and SeNPs, Se@OTV showed effective capacity to inhibit H1N1-induced segregation of erythrocytes (Figure 7A). This indicated that Se@OTV prevented interaction of the virus with MDCK cells. Untreated or Se@OTV-treated H1N1 was used to detect NA enzymatic activity.

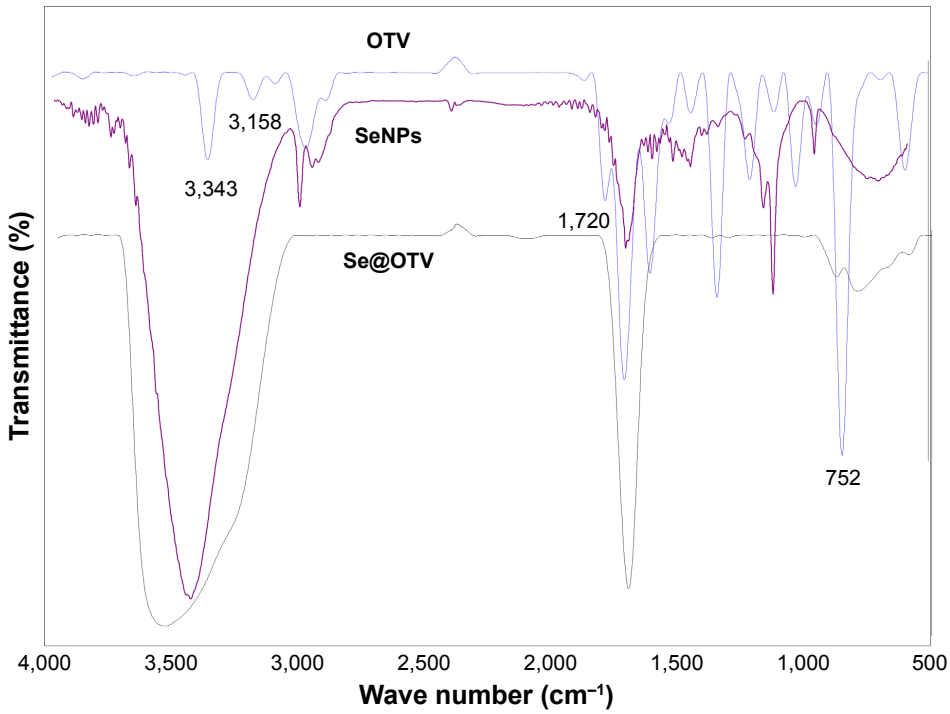

Figure 3 FTIR spectra of OTV, SeNPs, and Se@OTV. All IR spectra were acquired in the form of KBr plates.
Abbreviations: FTIR, Fourier-transform infrared; SeNPs, selenium nanoparticles; OTV, oseltamivir; Se@OTV, OTV SeNPs.

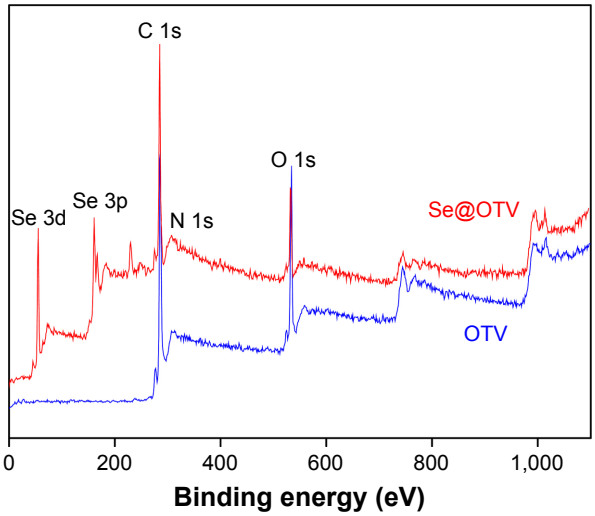

Figure 4 X-ray photoelectron spectroscopy of OTV and Se@OTV.
Abbreviations: OTV, oseltamivir; Se@OTV, OTV selenium nanoparticles.

Compared to OTV and SeNPs, Se@OTV had remarkable enzymatic activity, indicating that Se@OTV had an effect on NA activity (Figure 7B). A mechanism of anti-influenza activity by Se@OTV is postulated: Se@OTV bind to NA and HA activity, forbidding the attachment of H1N1 to MDCK cells.

Inhibition of H1N1 infection

MDCK cells exhibited typical apoptotic features, with H1N1 showing nuclear condensation and DNA fragmentation (Figure 8). Cotreatment with Se@OTV remarkably prevented H1N1-induced changes in nuclear morphology. These results revealed that Se@OTV rescued the apoptosis of MDCK cells by H1N1.

Inhibition of caspase-3 activation

Caspase 3 and PARP were used to determine cell apoptosis. The treatment of MDCK cells with H1N1 remarkably increased the activity of caspase 3 to 360%, as shown in Figure 9A. OTV and SeNPs slightly inhibited caspase-3 activity to 260% and 200%, respectively. However, Se@OTV significantly decreased caspase-3 activity to 115%. Compared to OTV and SeNPs, Se@OTV remarkably decreased protein-expression levels of PARP and caspase 3 (Figure 9B). The results show that Se@OTV inhibited H1N1 activity.

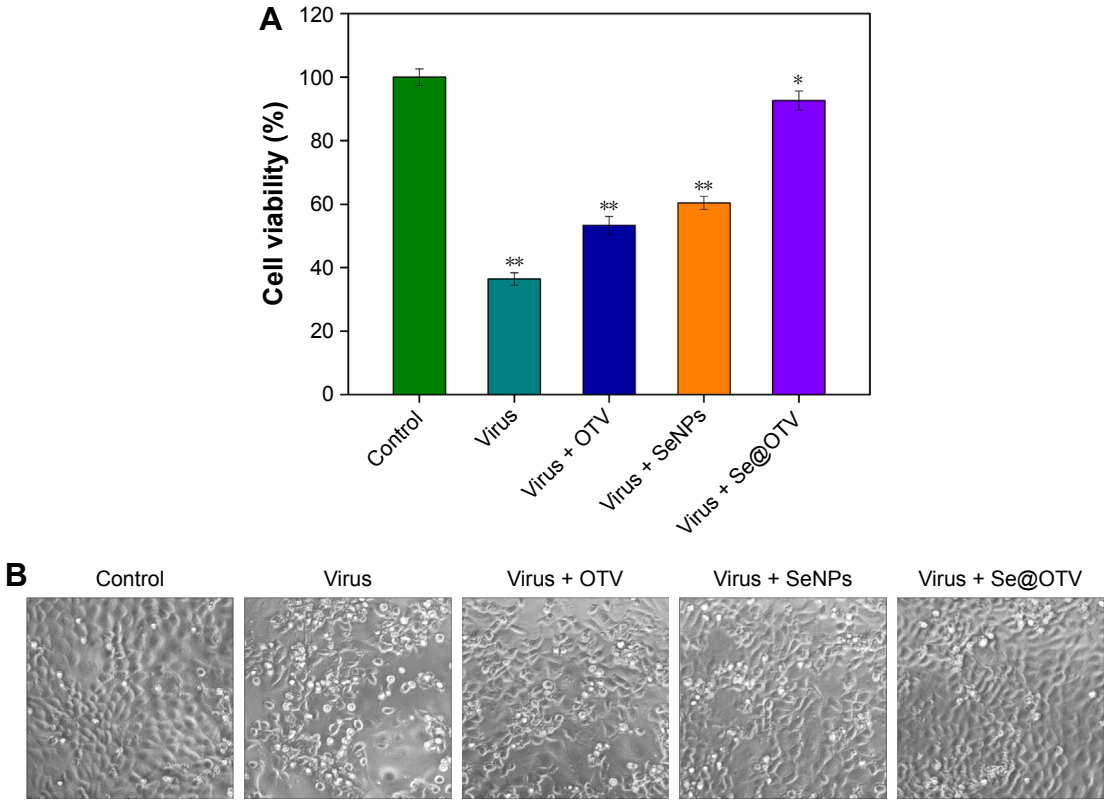

Figure 5 Effects of Se@OTV on the growth of H1N1 infection of MDCK cells by MTT assay.
Notes: (**A**) Antiviral activity of Se@OTV. Concentration of SeNPs was 1 mM and OTV 1 nM. (**B**) Morphological changes in H1N1-infected MDCK cells observed by phase-contrast microscopy. Bars with different characters are statistically different at *$P<0.05$ or **$P<0.01$ level.
Abbreviations: SeNPs, selenium nanoparticles; OTV, oseltamivir; Se@OTV, OTV SeNPs.

Table 1 The Reed–Münch assay was used to test the titer of H1N1 ($TCID_{50}=10^{3.6}$)

Dilution of H1N1	CPE	No CPE	Accumulation		Ratio CPE (%)
			CPE	No CPE	
10^{-1}	8	0	25	0	100 (25/25)
10^{-2}	8	0	17	0	100 (17/17)
10^{-3}	6	2	9	2	81.8 (9/11)
10^{-4}	3	5	3	7	30 (3/10)
10^{-5}	0	8	0	15	0 (0/15)

Abbreviations: $TCID_{50}$, 50% tissue-culture infective dose; CPE, cytopathic effect.

TEM of thin cell sections

As shown in Figure 10A, microvilli and mitochondria were observed with no morphological changes in untreated cells. When incubated with H1N1, TEM indicated a shrinking cytoplasm, distorted organelles, and condensed chromatin, which indicated apoptosis of MDCK cells (Figure 10B). The mitochondria of MDCK cells recovered their shape after treatment with Se@OTV, indicating that H1N1 induced apoptosis (Figure 10C).

Inhibition of ROS generation by Se@OTV

ROS generation was monitored through DCF assay to indicate the action mechanisms of Se@OTV. Intracellular ROS generation treated with H1N1 increased to 380%, as shown in Figure 11A. OTV and SeNPs slightly inhibited ROS generation to 270% and 210%, respectively. However, Se@OTV markedly decreased ROS generation (120%). The fluorescence intensity of DCF was found using H1N1, as shown in Figure 11B. The fluorescence intensity of DCF

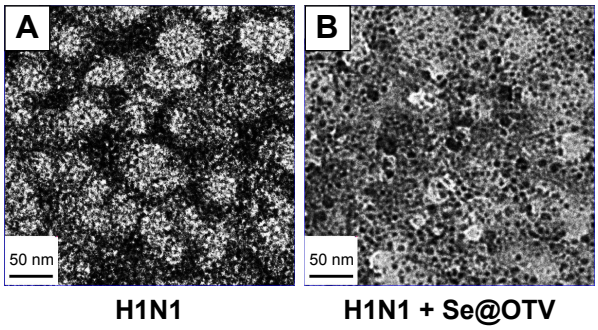

Figure 6 Morphologic abnormalities in Se@OTV-treated H1N1: high-resolution TEM negative staining.
Notes: (**A**) H1N1 virus control; (**B**) H1N1 virus interacting with Se@OTV. The combination concentration of Se in Se@OTV was 125 μM. The combination concentration of OTV in Se@OTV was 0.3 nM.
Abbreviations: OTV, oseltamivir; Se@OTV, OTV selenium nanoparticles; TEM, transmission electron microscopy.

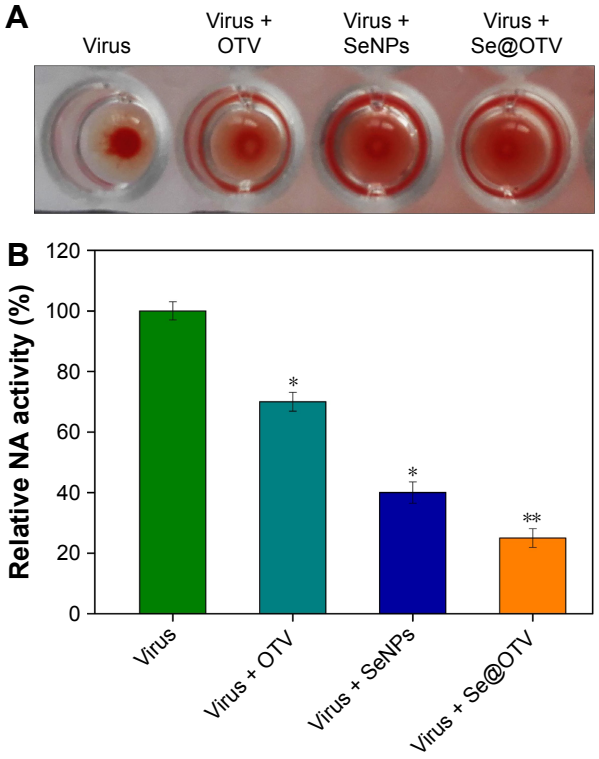

Figure 7 HA as potential target of Se@OTV.
Notes: (**A**) Comparisons of SeNP, OTV, and Se@OTV behavior in inhibition of influenza virus-induced aggregation of chicken erythrocytes. (**B**) NA-inhibition assay, performed utilizing NAs from H1N1 virus. Influenza virus NA activity was determined by quantifying fluorescence. The combination concentration of Se in Se@OTV was 125 μM. The combination concentration of OTV in Se@OTV was 0.3 nM. The concentration of free SeNPs was 1 mM. The concentration of free OTV was 1 nM. Bars with different characters are statistically different at $^{*}P<0.05$ or $^{**}P<0.01$ level.
Abbreviations: HA, hemagglutinin; NA, neuraminidase; SeNP, selenium nanoparticle; OTV, oseltamivir; Se@OTV, OTV SeNPs.

treated with H1N1 was much stronger than Se@OTV. These results indicate the role of ROS in antiviral action.

ROS activates apoptotic signaling pathways by Se@OTV

The overexpression of ROS could lead to DNA damage through regulation of apoptosis signaling pathways. As shown in Figure 12A, compared to OTV and SeNPs, treatments of MDCK cells with Se@OTV obviously inhibited the expression level of p53. Meanwhile, level of Akt was significantly increased by Se@OTV (Figure 12B). Taken together, the results indicate that Se@OTV depressed H1N1-induced host-cells apoptosis by ROS-mediated p53- and Akt-signaling pathways (Figure 12C).

Conclusion

In summary, we demonstrated an efficient chemical method through Se@OTV in this study. Se@OTV exhibits enhanced

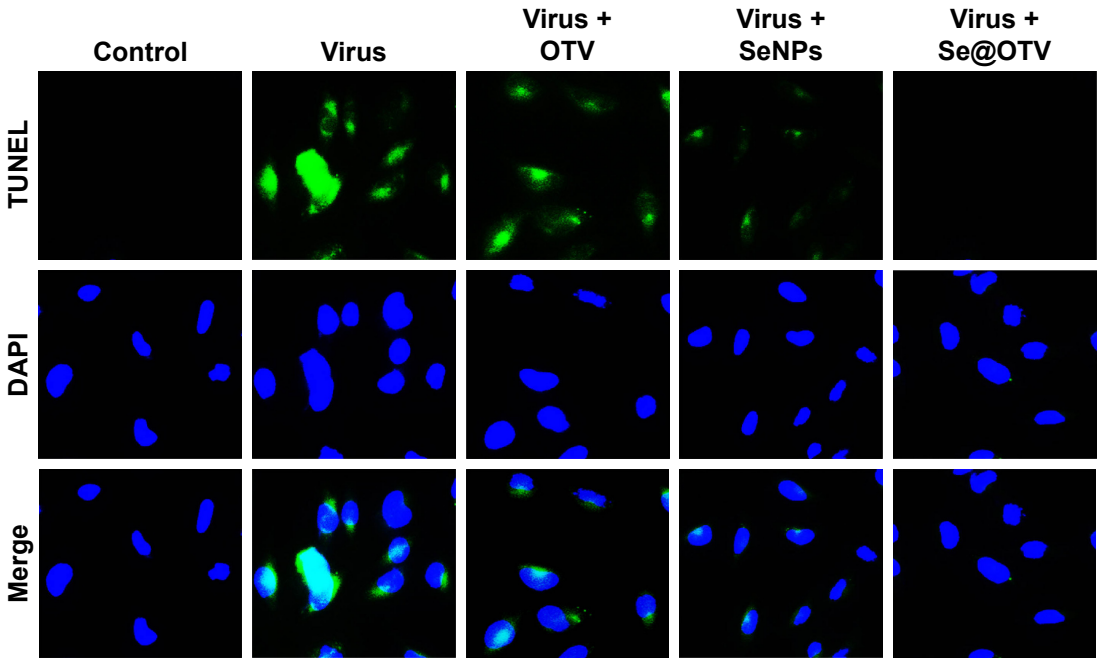

Figure 8 Se@OTV-induced apoptosis in H1N1 infection of MDCK cells.
Notes: DNA fragmentation and nuclear condensation detected by TUNEL–DAPI costaining assay. All results are representative of three independent experiments. The combination concentration of Se in Se@OTV was 125 μM. The combination concentration of OTV in Se@OTV was 0.3 nM. The concentration of free SeNPs was 1 mM. The concentration of free OTV was 1 nM.
Abbreviations: OTV, oseltamivir; SeNPs, selenium nanoparticles; Se@OTV, OTV SeNPs.

ability to prevent H1N1 infection and lower toxicity. Se@OTV interfered with H1N1 in MDCK through inhibition of HA and NA activity. The underlying molecular mechanisms verified that Se@OTV inhibited caspase 3-mediated apoptosis through ROS generation. More importantly, Se@OTV inhibited MDCK-cell apoptosis through regulating the level of ROS to trigger Akt and p53 pathways. Therefore, the nanosystem of Se@OTV might provide a prospective selenium species with antiviral properties against multidrug resistance.

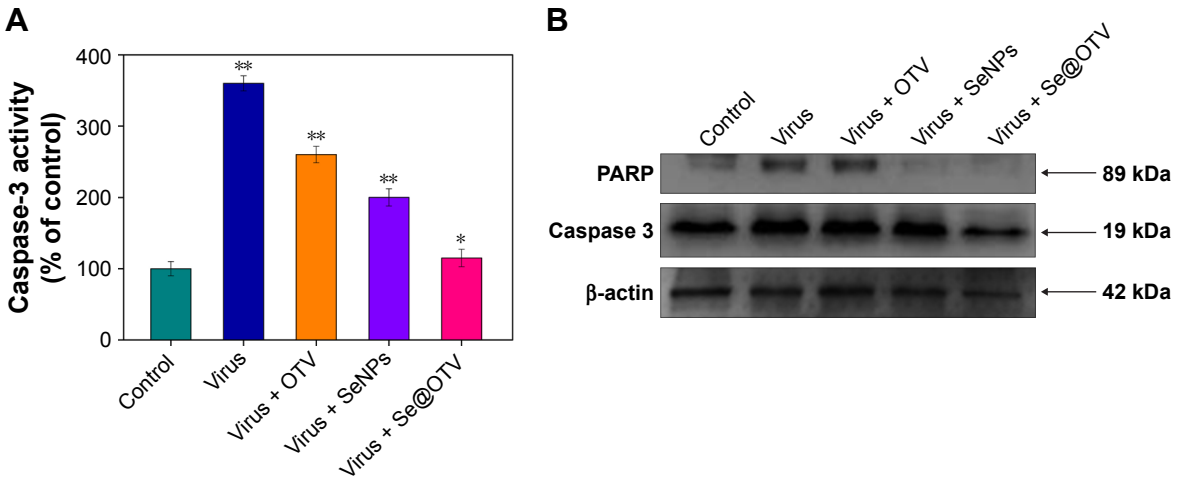

Figure 9 Inhibition of PARP cleavage and caspase-3 activity by Se@OTV in H1N1 infection of cells.
Notes: (**A**) Cells were treated with Se@OTV and caspase-3 activity detected by synthetic fluorogenic substrate; (**B**) protein expression of PARP and caspase 3 by Western blot, β-actin used as loading control. The combination concentration of Se in Se@OTV was 125 μM. The combination concentration of OTV in Se@OTV was 0.3 nM. The concentration of free SeNPs was 1 mM. The concentration of free OTV was 1 nM. Bars with different characters are statistically different at $^{*}P<0.05$ or $^{**}P<0.01$ level.
Abbreviations: OTV, oseltamivir; SeNPs, selenium nanoparticles; Se@OTV, OTV SeNPs.

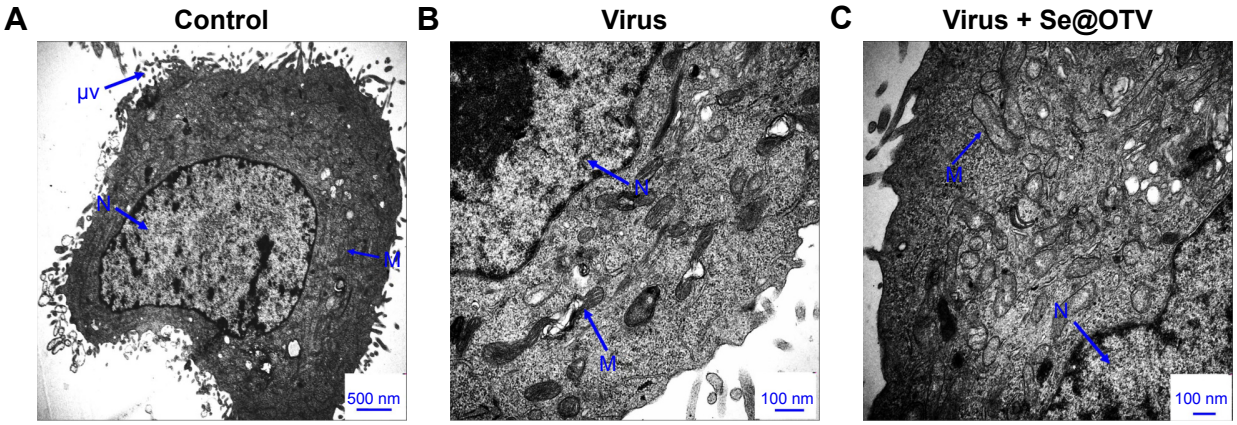

Figure 10 (**A**–**C**) TEM of thin sections of MDCK cells treated with different groups.
Notes: The combination concentration of Se in Se@OTV was 125 μM. The combination concentration of OTV in Se@OTV was 0.3 nM.
Abbreviations: TEM, transmission electron microscopy; SeNPs, selenium nanoparticles; OTV, oseltamivir; Se@OTV, OTV SeNPs; N, nucleus; M, mitochondria; Mv, microvilli.

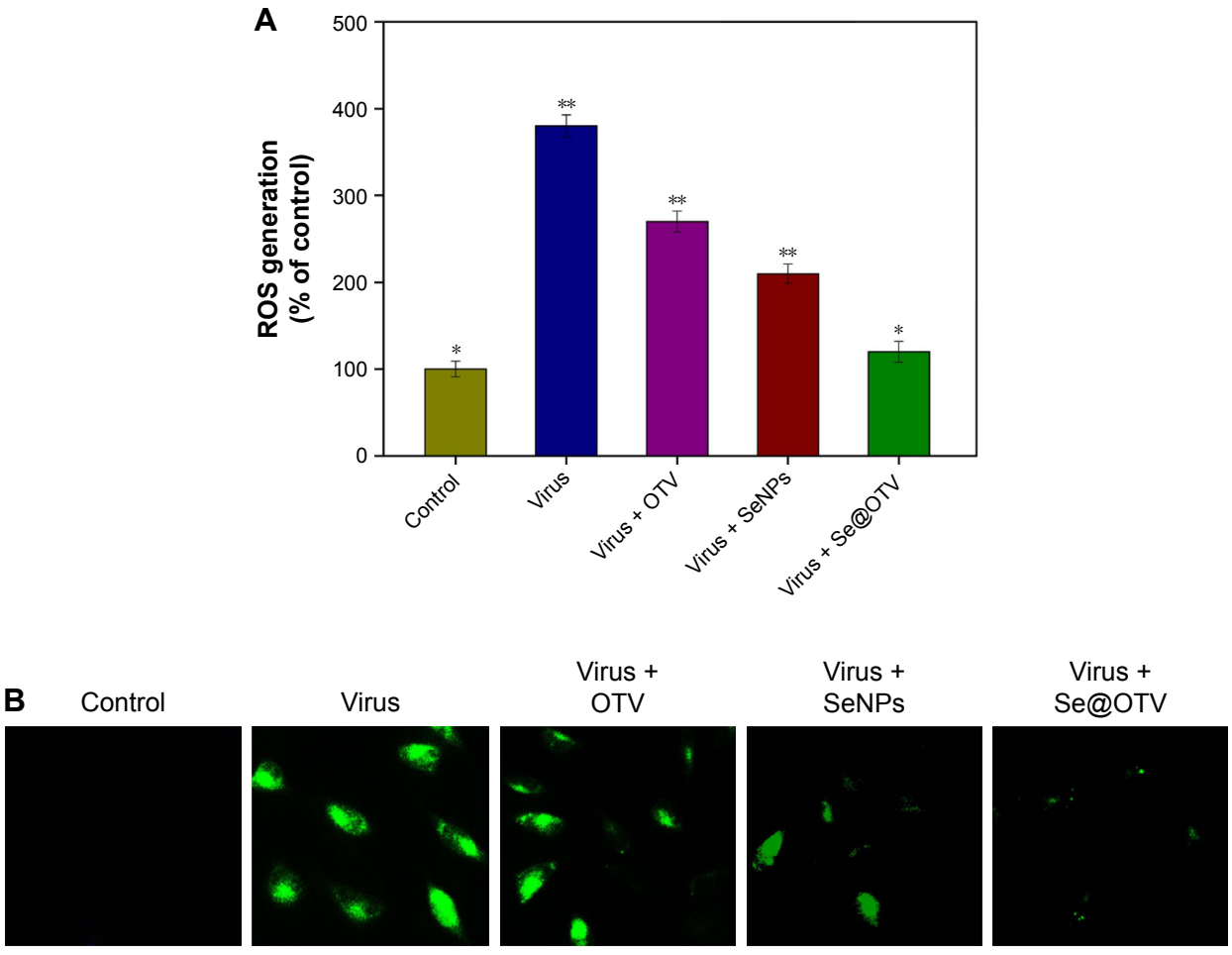

Figure 11 ROS overproduction induced by Se@OTV in H1N1 infection of MDCK cells.
Notes: (**A**) ROS levels were detected by DCF fluorescence intensity. (**B**) H1N1 infection of MDCK cells preincubated with 10 μM DCF for 30 minutes and then treated with Se@OTV. The combination concentration of Se in Se@OTV was 125 μM. The combination concentration of OTV in Se@OTV was 0.3 nM. The concentration of free SeNPs was 1 mM. The concentration of free OTV was 1 nM. Bars with different characters are statistically different at $^{*}P<0.05$ or $^{**}P<0.01$ level.
Abbreviations: ROS, reactive oxygen species; OTV, oseltamivir; SeNPs, selenium nanoparticles; Se@OTV, OTV SeNPs; DCF, dichlorofluorescein.

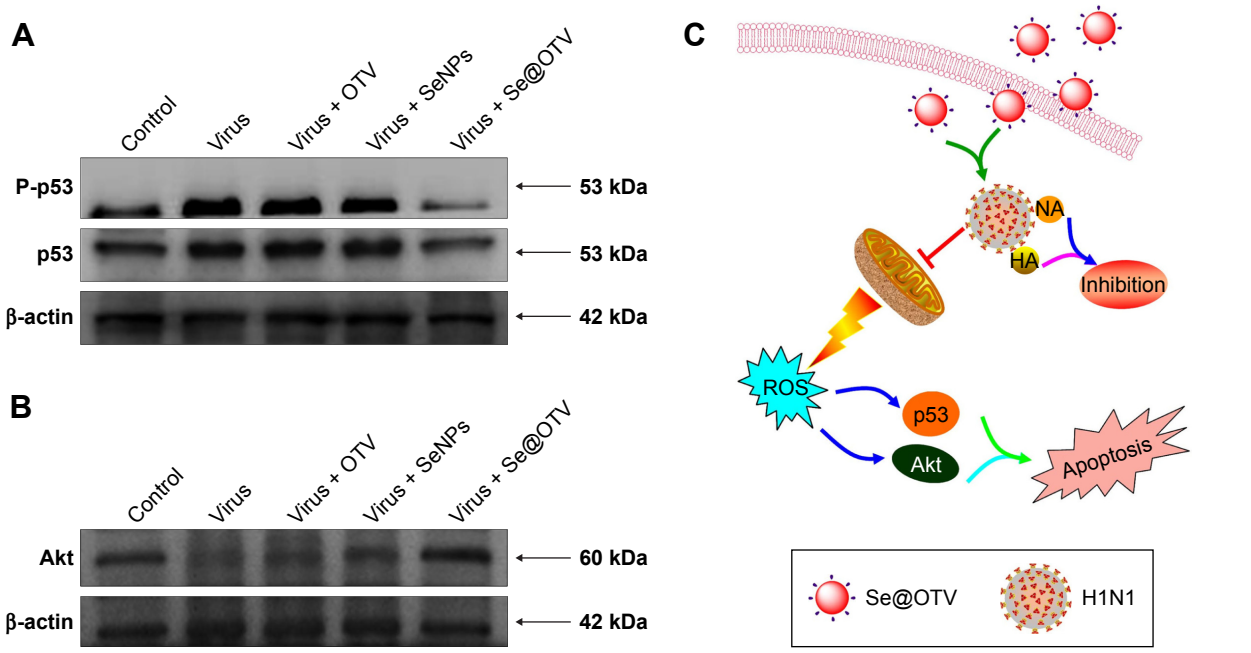

Figure 12 Intracellular apoptotic signaling pathways by Se@OTV in H1N1 infection of MDCK cells.
Notes: (**A**) Activation of p53-signaling pathway; (**B**) phosphorylation status-expression levels of Akt pathways; (**C**) main signaling pathway of ROS-mediated Akt- and p53-signaling pathways. The combination concentration of Se in Se@OTV was 125 μM. The combination concentration of OTV in Se@OTV was 0.3 nM. The concentration of free SeNPs was 1 mM. The concentration of free OTV was 1 nM.
Abbreviations: OTV, oseltamivir; SeNPs, selenium nanoparticles; Se@OTV, OTV SeNPs; ROS, reactive oxygen species.

Acknowledgments

This work was supported by the China Postdoctoral Science Foundation (2015M582366), the Technology Planning Project of Guangdong Province (2014A020212697), the Technology Planning Project of Guangdong (201607010120), and the Technology Planning Project of Guangzhou (2018-1002-SF-0673)

Disclosure

The authors report no conflicts of interest in this work.

References

1. Li YH, Lin ZF, Zhao MQ, et al. Silver nanoparticle based codelivery of oseltamivir to inhibit the activity of the H1N1 influenza virus through ROS-mediated signaling pathways. *ACS Appl Mater Interfaces*. 2016; 8(37):24385–24393.
2. Papp I, Sieben C, Ludwig K, et al. Inhibition of influenza virus infection by multivalent sialic-acid-functionalized gold nanoparticles. *Small*. 2010;6(24):2900–2906.
3. Tao WQ, Hurst BL, Shakya AK, et al. Consensus M2e peptide conjugated to gold nanoparticles confers protection against H1N1, H3N2 and H5N1 influenza A viruses. *Antiviral Res*. 2017;141:62–72.
4. Yang J, Shim SM, Nguyen TQ, et al. Poly-γ-glutamic acid/chitosan nanogel greatly enhances the efficacy and heterosubtypic cross-reactivity of H1N1 pandemic influenza vaccine. *Sci Rep*. 2017;7:44839.
5. Li YH, Lin ZF, Zhao MQ, et al. Reversal of H1N1 influenza virus-induced apoptosis by silver nanoparticles functionalized with amantadine. *RSC Adv*. 2016;6(92):89679–89686.
6. Loveday EK, Diederich S, Pasick J, Jean F. Human microRNA-24 modulates highly pathogenic avian-origin H5N1 influenza A virus infection in A549 cells by targeting secretory pathway furin. *J Gen Virol*. 2015; 96(Pt 1):30–39.
7. Madrahimov A, Helikar T, Kowal B, Lu GQ, Rogers J. Dynamics of influenza virus and human host interactions during infection and replication cycle. *B Math Biol*. 2013;75(6):988–1011.
8. Londrigan SL, Short KR, Ma J, et al. Infection of mouse macrophages by seasonal influenza viruses can be restricted at the level of virus entry and at a late stage in the virus life cycle. *J Virol*. 2015;89(24): 12319–12329.
9. Lin ZF, Li YH, Guo M, et al. The inhibition of H1N1 influenza virus-induced apoptosis by silver nanoparticles functionalized with zanamivir. *RSC Adv*. 2017;7(2):742–750.
10. Lauster D, Glanz M, Bardua M, et al. Multivalent peptide-nanoparticle conjugates for influenza-virus inhibition. *Angew Chem Int Ed Engl*. 2017;56(21):5931–5936.
11. Xiao SL, Si LL, Tian ZY, et al. Pentacyclic triterpenes grafted on CD cores to interfere with influenza virus entry: a dramatic multivalent effect. *Biomaterials*. 2016;78:74–85.
12. Chou TC, Hsu W, Wang CH, Chen YJ, Fang JM. Rapid and specific influenza virus detection by functionalized magnetic nanoparticles and mass spectrometry. *J Nanobiotechnology*. 2011;9:52.
13. Choi JY, Martin SJ, Tripp RA, Tompkins SM, Dluhy RA. Detection of neuraminidase stalk motifs associated with enhanced N1 subtype influenza A virulence via Raman spectroscopy. *Analyst*. 2015; 140(22):7748–7760.
14. Kristensen AB, Lay WN, Ana-Sosa-Batiz F, et al. Antibody responses with Fc-mediated functions after vaccination of HIV-infected subjects with trivalent influenza vaccine. *J Virol*. 2016;90(12):5724–5734.
15. Xiang DX, Zheng Y, Duan W, et al. Inhibition of A/human/Hubei/3/2005 (H3N2) influenza virus infection by silver nanoparticles in vitro and in vivo. *Int J Nanomedicine*. 2013;8:4103–4713.
16. Yu M, Wang Y, Tian L, et al. Safflomin A inhibits neuraminidase activity and influenza virus replication. *RSC Adv*. 2015;5(114):94053–94066.
17. Abed Y, Carbonneau J, L'Huillier AG, Kaiser L, Boivin G. Droplet digital PCR to investigate quasi-species at codons 119 and 275 of the A(H1N1)pdm09 neuraminidase during zanamivir and oseltamivir therapies. *J Med Virol*. 2017;89(4):737–741.

18. Neri-Bazán RM, García-Machorro J, Méndez-Luna D, et al. Design, in silico studies, synthesis and in vitro evaluation of oseltamivir derivatives as inhibitors of neuraminidase from influenza A virus H1N1. *Eur J Med Chem*. 2017;128:154–167.
19. Nguyen JT, Smee DF, Barnard DL, et al. Efficacy of combined therapy with amantadine, oseltamivir, and ribavirin in vivo against susceptible and amantadine-resistant influenza A viruses. *PloS One*. 2012;7(1):e31006.
20. Bronstein LM. Virus-based nanoparticles with inorganic cargo: what does the future hold? *Small*. 2011;7(12):1609–1618.
21. Jackman JA, Lee J, Cho NJ. Nanomedicine for infectious disease applications: innovation towards broad-spectrum treatment of viral infections. *Small*. 2016;12(9):1133–1139.
22. Baram-Pinto D, Shukla S, Gedanken A, Sarid R. Inhibition of HSV-1 attachment, entry, and cell-to-cell spread by functionalized multivalent gold nanoparticles. *Small*. 2010;6(9):1044–1050.
23. Tao W, Hurst BL, Shakya AK, et al. Consensus M2e peptide conjugated to gold nanoparticles confers protection against H1N1, H3N2 and H5N1 influenza A viruses. *Antiviral Res*. 2017;141:62–72.
24. Vonnemann J, Sieben C, Wolff C, et al. Virus inhibition induced by polyvalent nanoparticles of different sizes. *Nanoscale*. 2014;6(4):2353–2360.
25. Sokolova V, Westendorf AM, Buer J, Uberla K, Epple M. The potential of nanoparticles for the immunization against viral infections. *J Mater Chem B Mater Biol Med*. 2015;3(24):4767–4779.
26. Wang J, Zhu RR, Gao B, et al. The enhanced immune response of hepatitis B virus DNA vaccine using SiO2@LDH nanoparticles as an adjuvant. *Biomaterials*. 2014;35(1):466–478.
27. Shen LH, Zhou J, Wang YX, et al. Efficient encapsulation of Fe_3O_4 nanoparticles into genetically engineered hepatitis B core virus-like particles through a specific interaction for potential bioapplications. *Small*. 2015;11(9–10):1190–1196.
28. Zhang R, Lin Z, Lui VC, et al. Silver nanoparticle treatment ameliorates biliary atresia syndrome in rhesus rotavirus inoculated mice. *Nanomedicine*. 2017;13(3):1041–1050.
29. Stevanović M, Filipović N, Djurdjević J, Lukić M, Milenković M, Boccaccini A. 45S5 Bioglass-based scaffolds coated with selenium nanoparticles or with poly(lactide-co-glycolide)/selenium particles: processing, evaluation and antibacterial activity. *Colloids Surf B Biointerfaces*. 2015;132:208–215.
30. Ramya S, Shanmugasundaram T, Balagurunathan R. Biomedical potential of actinobacterially synthesized selenium nanoparticles with special reference to anti-biofilm, anti-oxidant, wound healing, cytotoxic and anti-viral activities. *J Trace Elem Med Biol*. 2015;32:30–39.
31. Harthill M. Review: micronutrient selenium deficiency influences evolution of some viral infectious diseases. *Biol Trace Elem Res*. 2011;143(3):1325–1336.
32. Erkekoğlu P, Aşçi A, Ceyhan M, et al. Selenium levels, selenoenzyme activities and oxidant/antioxidant parameters in H1N1-infected children. *Turk J Pediatr*. 2013;55(3):271–282.
33. Li YH, Li XL, Wong YS, et al. The reversal of cisplatin-induced nephrotoxicity by selenium nanoparticles functionalized with 11-mercapto-1-undecanol by inhibition of ROS-mediated apoptosis. *Biomaterials*. 2011;32(34):9068–9076.
34. Bai KK, Hong BH, He JL, Hong ZA, Tan R. Preparation and antioxidant properties of selenium nanoparticles-loaded chitosan microspheres. *Int J Nanomedicine*. 2017;12:4527–4539.
35. Li YH, Lin ZF, Zhao MQ, et al. Multifunctional selenium nanoparticles as carriers of HSP70 siRNA to induce apoptosis of HepG2 cells. *Int J Nanomedicine*. 2016;11:3065–3076.
36. Li YH, Li XL, Zheng WJ, Fan CD, Zhang YB, Chen TF. Functionalized selenium nanoparticles with nephroprotective activity, the important roles of ROS-mediated signaling pathways. *J Mater Chem B Mater Biol Med*. 2013;1(46):6365–6372.
37. Yang F, Tang QM, Zhong XY, et al. Surface decoration by *Spirulina* polysaccharide enhances the cellular uptake and anticancer efficacy of selenium nanoparticles. *Int J Nanomedicine*. 2012;7:835–844.
38. Yu L, Sun L, Nan Y, Zhu LY. Protection from H1N1 influenza virus infections in mice by supplementation with selenium: a comparison with selenium-deficient mice. *Biol Trace Elem Res*. 2011;141(1–3):254–261.
39. Cheng ZK, Zhi XG, Sun G, et al. Sodium selenite suppresses hepatitis B virus transcription and replication in human hepatoma cell lines. *J Med Virol*. 2016;88(4):653–663.
40. Huang YY, Luo Y, Zheng WJ, Chen TF. Rational design of cancer-targeted BSA protein nanoparticles as radiosensitizer to overcome cancer radioresistance. *ACS Appl Mater Interfaces*. 2014;6(21):19217–19228.
41. Zhu B, Li YH, Lin ZF, et al. Silver nanoparticles induce HePG-2 cells apoptosis through ROS-mediated signaling pathways. *Nanoscale Res Lett*. 2016;11(1):198.
42. Li YH, Lin ZF, Xu TT, et al. Delivery of VP1 siRNA to inhibit the EV71 virus using functionalized silver nanoparticles through ROS-mediated signaling pathways. *RSC Adv*. 2017;7(3):1453–1463.
43. Liu W, Li XL, Wong YS, et al. Selenium Nanoparticles as a carrier of 5-fluorouracil to achieve anticancer synergism. *ACS Nano*. 2012;6(8):6578–6591.
44. Li YH, Guo M, Lin ZF, et al. Polyethylenimine-functionalized silver nanoparticle-based co-delivery of paclitaxel to induce HepG2 cell apoptosis. *Int J Nanomedicine*. 2016;11:6693–6702.
45. Xiang DX, Zheng Y, Duan W, et al. Inhibition of A/human/Hubei/3/2005 (H3N2) influenza virus infection by silver nanoparticles in vitro and in vivo. *Int J Nanomedicine*. 2013;8:4103–4113.
46. He LZ, Huang YY, Zhu HL, et al. Cancer-targeted monodisperse mesoporous silica nanoparticles as carrier of ruthenium polypyridyl complexes to enhance theranostic effects. *Adv Funct Mater*. 2014;24(19):2754–2763.
47. Huang YY, He LZ, Liu W, et al. Selective cellular uptake and induction of apoptosis of cancer-targeted selenium nanoparticles. *Biomaterials*. 2013;34(29):7106–7116.
48. Li JM, Wang YY, Zhao MX, et al. Multifunctional QD-based co-delivery of siRNA and doxorubicin to HeLa cells for reversal of multidrug resistance and real-time tracking. *Biomaterials*. 2012;33(9):2780–2790.
49. You YY, Hu H, He LZ, Chen TF. Differential effects of polymer-surface decoration on drug delivery, cellular retention, and action mechanisms of functionalized mesoporous silica nanoparticles. *Chem Asian J*. 2015;10(12):2743–2753.
50. Liu T, Zeng LL, Jiang WT, Fu YT, Zheng WJ, Chen TF. Rational design of cancer-targeted selenium nanoparticles to antagonize multidrug resistance in cancer cells. *Nanomedicine*. 2015;11(4):947–958.